A Computational Tool for Designing FRET Protein Biosensors by Rigid-Body Sampling of Their Conformational Space

Elizabeth Pham,[1] Jason Chiang,[1,2] Isaac Li,[1] Warren Shum,[2] and Kevin Truong[1,2,*]

[1] Institute of Biomaterials and Biomedical Engineering, University of Toronto, 164 College Street, Toronto, Ontario M5S 3G9, Canada
[2] Edward S. Rogers, Sr. Department of Electrical and Computer Engineering, University of Toronto, 10 King's College Circle, Toronto, Ontario M5S 3G4, Canada
*Correspondence: kevin.truong@utoronto.ca

SUMMARY

Biosensors relying on the fluorescence resonance energy transfer (FRET) between fluorescent proteins have been used for live-cell imaging of cellular events including Ca^{2+} signaling. The efficiency of energy transfer between the donor and acceptor fluorescent proteins depends on the relative distance and orientation between them, which become altered by conformational changes of a fused sensory protein caused by a cellular event. In this way, changes in FRET efficiency of Ca^{2+} biosensors can be correlated with Ca^{2+} concentrations. The design of these FRET biosensors can be improved by modeling conformational changes before and after a cellular event. Hence, a computational tool called FPMOD was developed to predict FRET efficiency changes by constructing FRET biosensors and sampling their conformational space through rigid-body rotation. We showed with FPMOD that our computational modeling approach can qualitatively predict the FRET efficiencies of a range of biosensors, which had strong agreement with experimental results.

Introduction

Fluorescence resonance energy transfer (FRET) biosensors have become invaluable tools for the live-cell imaging of many cellular events such as caspase activation, protein phosphorylation, and Ca^{2+} signaling (Griesbeck, 2004; Miyawaki, 2003; Pozzan et al., 2003; Truong and Ikura, 2001). FRET is the natural phenomenon of energy transfer via resonance between two fluorophores with a spectral overlap between the donor emission and the acceptor excitation. The efficiency of this energy transfer dynamically responds to the relative distance and orientation between the donor and acceptor (Clegg, 1995). In FRET biosensors, natural sensory proteins for the desired cellular events are inter- or intramolecularly fused with

a pair of fluorescent proteins suitable for FRET, such as cyan fluorescent protein (CFP) as the donor and yellow fluorescent protein (YFP) as the acceptor (Li et al., 2006; Tsien, 1998). The conformational change of the sensory protein caused by the cellular event alters the distance and orientation of the fluorescent proteins. Hence, a change in FRET efficiency of the biosensor is correlated with the cellular event. For example, FRET Ca^{2+} biosensors have been designed that correlate Ca^{2+} concentration levels with FRET efficiency changes between CFP and YFP genetically fused with Calmodulin (CaM), a cytoplasmic Ca^{2+}-sensitive protein (Berridge et al., 2000; Miyawaki et al., 1997, 1999). Upon binding Ca^{2+} ions, CaM undergoes a conformational change from an extended to a more compact conformation by wrapping around a CaM-binding peptide such as that from myosin light chain kinase (MLCKp) (Kuboniwa et al., 1995; Wriggers et al., 1998). This conformational change alters the relative distance and orientation of the fluorescent proteins. As a result, an increase in FRET efficiency is correlated with a higher Ca^{2+} concentration. By observing the change in fluorescence intensity of the acceptor YFP, the onset and termination of localized Ca^{2+} signaling can be detected. To accurately distinguish signal from noise, these biosensors often need a large dynamic range, which is defined as the division of the maximum emission ratio (R_{max}) by the minimum emission ratio (R_{min}), where the emission ratio is the quotient of the acceptor emission peak to the donor emission peak. One common approach to improving dynamic range is by using variants of CFP and YFP that have more favorable properties for FRET such as Cerulean, Citrine, Venus, and circularly permutated fluorescent proteins (Griesbeck et al., 2001; Miyawaki et al., 1999; Nagai et al., 2002; Rekas et al., 2002).

The design of FRET biosensors can be improved by modeling their conformational changes before and after activation by a cellular event. For example, a FRET Ca^{2+} biosensor with an improved dynamic range was rationally designed based on the NMR structure of CaM bound to the CaM-binding peptide from CaM-dependent kinase kinase (CKKp) (Truong et al., 2001). The computational model of the CaM and CKKp complex showed that CKKp could be spliced within the hinge of CaM. This allowed for

a reduced distance between the fluorescent proteins in the Ca^{2+}-bound form of the biosensor, resulting in a higher R_{max} and, thus, a larger dynamic range. In another example, the dynamic range of a caspase-3 activation biosensor was improved by computational modeling based on the solved atomic structure of caspase-3 bound to its tetrapeptide inhibitor (Xu et al., 1998). Caspase-3 proteolytic cleavage of its specific target sequences within substrate proteins is a key activating event of apoptosis. To image caspase-3 activation in living cells, a biosensor can be constructed consisting of a fusion of a CFP donor, a specific cleavage recognition sequence, and a YFP acceptor. Computational modeling showed that the optimal linker length of a caspase-3 activation biosensor was 20 amino acid residues (Chiang and Truong, 2006). The optimization of this linker length produced a biosensor with a greater dynamic range for both in vitro and in vivo studies. These examples demonstrate the effectiveness of designing a FRET biosensor by studying its conformational changes. Hence, in this paper, we describe a computational tool called FPMOD (Fusion Protein Modeler; available at http://individual.utoronto.ca/ktruong/software.htm) to construct FRET biosensors and sample conformational spaces for the purpose of predicting FRET efficiency changes. FPMOD consists of a set of programs used to generate fusion protein constructs from PDB files, to define regions of flexible linkers between domains, and to produce random conformations by rotation of domains around these flexible linkers. For each conformation generated, the distance and orientation factors, as well as FRET efficiencies, are then calculated. A tabulation of these values can be used to predict FRET changes of biosensor designs. To demonstrate the feasibility of FPMOD, it was used to predict FRET efficiency changes, as well as corresponding emission-ratio changes, which had a strong agreement with experimental results, of several FRET Ca^{2+} biosensors. Changes in FRET signals for ten different experimentally generated biosensor constructs were determined. In all cases, qualitative predictions of the FRET signal decrease or increase agreed with experimental findings.

Results and Discussion

Understanding the conformational space conferred by flexible linkers is important for predicting the FRET efficiency changes of biosensors in response to a stimulus. We introduced a modeling tool called FPMOD that is capable of constructing fusion proteins given solved atomic structures of the individual protein domains. More importantly, FPMOD was used to sample the conformational space of these fusion proteins by treating each domain as a rigid body and rotating the domains with respect to their flexible linkers. The dihedral angles ψ and φ take on random values, and conformations that do not sterically collide after random rotations of the linker regions are accepted. With this approximation, no preferences are given to particular dihedral angles or any potentially favorable packing of rigid domains. It is possible that using a gradient of linker flexibility may provide a better correlation between simulated and experimental results by eliminating certain less favorable conformations. However, for simplicity, in FPMOD, the intervening linker regions between user-defined boundaries are given complete flexibility. Surprisingly, even with these relatively crude approximations, it was sufficient to detect a qualitative correlation between simulation and experimental results.

Besides approximations incorporated into the simulation process, possible sources of error exist for the experimental values obtained. Photobleaching of fluorophores, protein degradation, and autofluorescence interfering with spectral data are common concerns. In addition, fluorophore properties may be altered when they are part of fusion proteins. While these experimental sources of error were not significant enough to prevent a qualitative correlation, they may contribute to discrepancies between quantitative comparisons.

The Relationship between the Changes in FRET Efficiency and FRET Emission Ratio

FRET efficiency changes are interpreted differently in the context of simulations versus experimental data. In simulating biosensor models, a change in FRET efficiency is simply the percentage increase or decrease in FRET efficiency values between two cases. However, experimentally, a change in FRET efficiency is evident as a change in emission spectra such that the emission ratio of YFP to CFP can be calculated. Thus, a means of estimating emission ratio from FRET efficiency has been developed (see Experimental Procedures) to translate FRET efficiency values found through simulation into emission ratios to allow for the direct comparison between theoretical and experimental results. In addition, the qualitative changes also serve as a means of comparison between these two sets of data in which an increase in FRET efficiency would be apparent in in vitro studies as an increase in the FRET emission ratio of YFP to CFP. Using this qualitative comparison, simulation results of FRET efficiency predictions were found to be consistent with in vitro experimental data in all tested cases (Table 1).

Ca^{2+} Biosensors Based on the CaM-MLCKp or CaM-CKKp Complex Show Both an Increase and Decrease, Respectively, in FRET Efficiency

Recently, we designed two CaM-based biosensors (named YCKKpC-CaM and YMLCKpC-CaM), and computational modeling with FPMOD showed that the FRET efficiency for YCKKpC-CaM should decrease, while that for YMLCKpC-CaM should increase, upon Ca^{2+} binding. The structural diversity of CaM-peptide binding was used to design two biosensors to measure Ca^{2+}-concentration changes in living cells. FPMOD simulation results predicted that the FRET efficiency for both biosensors would be similar in the unbound case, but suggested that while FRET efficiency would increase for YMLCKpC-CaM upon binding of Ca^{2+} from 17% to 32%, it would decrease for YCKKpC-CaM from 20% to 7.6%. This corresponds to a predicted emission-ratio increase of 45% and a decrease of 26%. Although in both cases CaM undergoes conformational changes upon Ca^{2+} induction, the resulting complexes are different (Figure 1). First, there

Table 1. Tabulation of the Distance Factor, Orientation Factor, and FRET Efficiency Values Predicted by FPMOD Simulation

	Distance[a] (Å)	κ^2	E%	Sim EmR	Exp EmR	Sim EmR Change (%)	Exp EmR Change (%)
Predicted Biosensor Cases							
YMLCKpC-CaM (unbound)	65 ± 13	0.77	17	1.07	1.5	—	—
YMLCKpC-CaM (bound)	50 ± 8.1	0.55	32	1.55	2.2	45	47
YCKKpC-CaM (unbound)	61 ± 15	0.64	20	1.15	2.1	—	—
YCKKpC-CaM (bound)	72 ± 13	0.40	7.6	0.85	1.7	−26	−19
YC21 (unbound)	75 ± 15	0.69	7.1	0.84	1.1	—	—
YC21 (bound)	75 ± 15	0.77	9.4	0.89	1.6	5.9	45
YC61 (unbound)	76 ± 15	0.59	6.9	0.83	1.1	—	—
YC61 (bound)	69 ± 15	0.70	12	0.95	2.3	14	109
CEcadY12 (unbound)	91 ± 21	0.59	3.1	0.76	0.81	—	—
CEcadY12 (bound)	85 ± 20	0.39	4.5	0.79	0.92	3.6	14
Predicted cpVenus Biosensor Cases							
cp49Venus (bound)	77 ± 13	0.76	7.2	0.84	1.4	0.25	0
cp157Venus (bound)	74 ± 14	0.86	9.5	0.89	2.8	6.2	158
cp173Venus (bound)	75 ± 18	0.82	11	0.92	4.3	10	210
cp195Venus (bound)	76 ± 17	0.90	8.3	0.86	2.4	3.0	102
cp229Venus (bound)	77 ± 13	0.76	7.3	0.85	1.75	1.3	75
cp58Venus (bound)	78 ± 19	0.51	9.8	0.88	—	4.9	—
cp116Venus (bound)	76 ± 15	0.90	7.5	0.85	—	1.0	—
cp135Venus (bound)	78 ± 15	0.59	7.4	0.84	—	0.75	—
cp145Venus (bound)	73 ± 15	0.69	8.4	0.87	—	3.3	—
cp215Venus (bound)	75 ± 14	0.67	9.1	0.88	—	5.1	—

[a] Errors provided for the distance factors calculated correspond to standard deviations of a sample with 130 models. Errors are not provided for the orientation factor and FRET efficiency values because they display non-Gaussian distributions.

is a structural difference between the target peptides when in complex with CaM, where MLCKp adopts an α-helical conformation and CKKp forms an α helix with a hairpin-like loop folded back onto the α helix. Second, the peptides bind to CaM in opposite orientations (Ikura et al., 1992; Osawa et al., 1999). Due to these differences, the direction of FRET efficiency change is different between the two biosensor constructs. In fact, in vitro experimental data confirmed the predicted direction of change, whether increasing or decreasing, showing an emission-ratio increase of 47% for YMLCKpC-CaM and a decrease of 19% for YCKKpC-CaM (Figures 2 and 3). Furthermore, simulation results predicted that unbound FRET efficiencies of YMLCKpC-CaM and YCKKpC-CaM are higher than that of YC2.1, with efficiency values of 17% and 20%, respectively, versus 7.1% (Table 1). These constructs have higher FRET efficiencies because the distance is closer structurally (65 Å for YMLCKpC-CaM and 61 Å for YCKKpC-CaM versus 75 Å for YC2.1). This prediction is consistent with experimental findings. The biosensors display both an increase and decrease in distance factor, but both show a decrease in orientation factor. Since the direction of efficiency change correlates with that of

distance change, the distance factor is the dominant influence in these biosensors.

The YC6.1 Ca²⁺ Biosensor Has a Larger Dynamic Range Than YC2.1

FPMOD also confirmed that the YC6.1 biosensor does indeed have a higher FRET efficiency than YC2.1. YC6.1 was previously designed based on the NMR structure of CaM bound to CKKp (Osawa et al., 1999) and was seen to display a 2-fold increase in the FRET dynamic range (Truong et al., 2001). Studies have shown that CaM binds to different target peptides through different mechanisms and interactions. Specifically, CaM binds to peptides MLCKp and CKKp in the presence of Ca²⁺ (Ikura et al., 1992; Osawa et al., 1999). YC2.1 was designed based on the structural information for CaM bound to MLCKp and consisted of the traditional tandem fusion of CFP, CaM, MLCKp, and YFP. However, structural studies of CaM bound to CKKp suggested an innovative design for a new biosensor (Truong et al., 2001). The unique binding of CaM to CKKp and the orientation of the peptide with respect to the two CaM domains suggested that CKKp could replace a linker region within the CaM protein itself. Thus, YC6.1, consisting of a tandem fusion of CFP, the
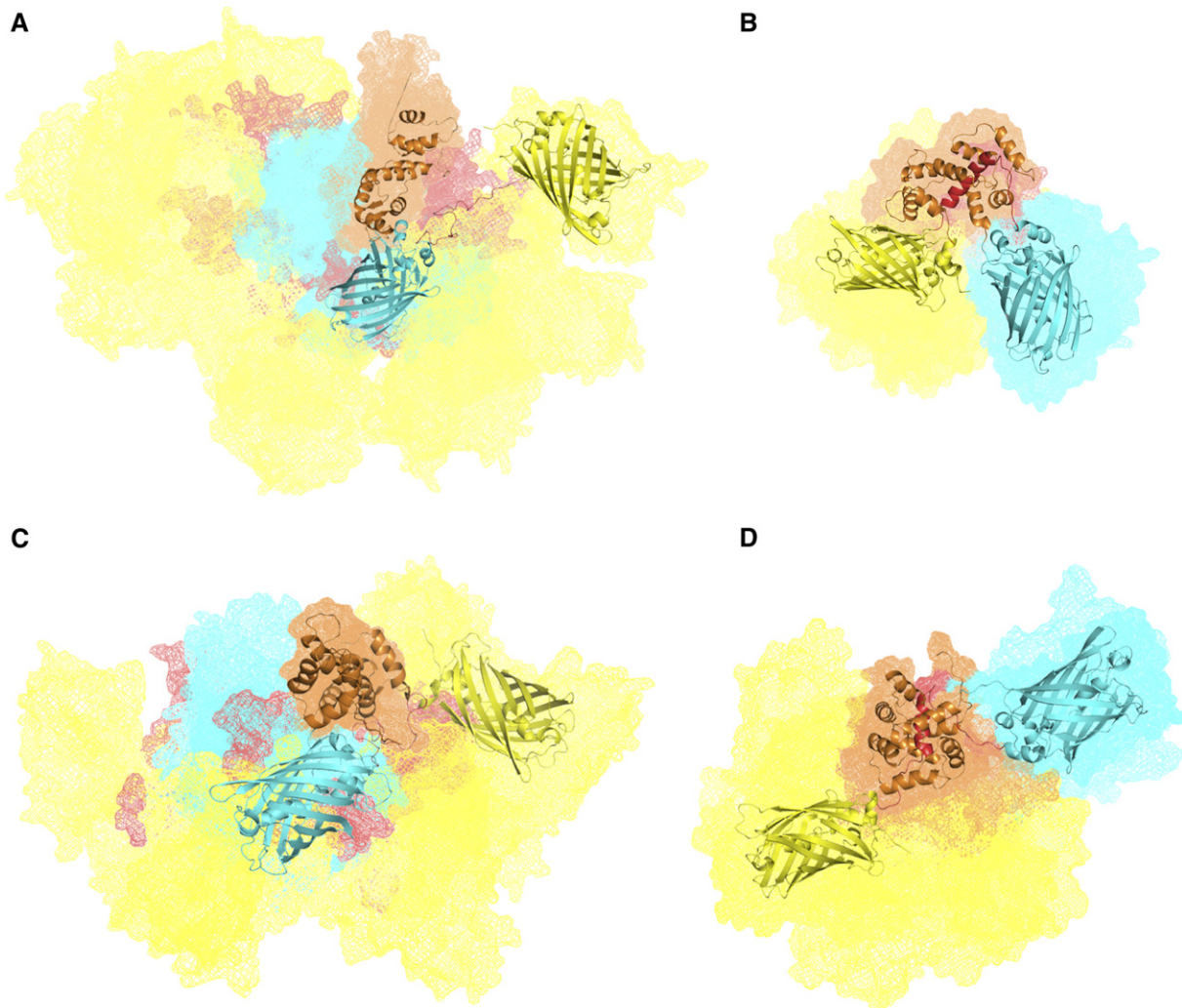
Figure 1. Superposition of Multiple Conformations of the YMLCKpC-CaM and YCKKpC-CaM Biosensors in the Presence and Absence of Ca^{2+} Binding

(A–D) Superposition of possible conformations for the YMLCKpC-CaM biosensor (A) before and (B) after Ca^{2+} binding and for the YCKKpC-CaM biosensor (C) before and (D) after Ca^{2+} binding. Before Ca^{2+} binding, conformations are in the unbound state and models are aligned with CaM; after Ca^{2+} binding, conformations are in the bound state and models are aligned with the CaM-peptide complex. Several conformations are highlighted for emphasis with CaM (orange), YFP (yellow), CFP (cyan), and CaM-binding peptide (red).

N-terminal fragment of CaM (N-CaM), CKKp as the linker region, the C-terminal fragment of CaM (C-CaM), and YFP, was constructed (Truong et al., 2001). It was assumed that the unbound forms of YC2.1 and YC6.1 would be separated by a similar distance and would thus have similar FRET efficiencies, but it was expected that YC6.1 would display a greater dynamic range since it would allow for a closer interaction, and thus a shorter distance, in the CaM-CKKp complex than the CaM-MLCKp complex of YC2.1. FPMOD confirmed that YC6.1 had a higher FRET efficiency change upon Ca^{2+} induction than YC2.1 (6.9% to 12% versus 7.1% to 9.4%), which corresponds to increases in emission ratios of 14% versus 5.9%. This is qualitatively consistent with in vitro data, which indicated emission-ratio increases of 109% and 45% for

YC6.1 and YC2.1, respectively (Truong et al., 2001). FPMOD results also confirmed that while the unbound distances were similar between YC6.1 and YC2.1 (76 Å versus 75 Å), YC6.1 was indeed a more compact complex with a shorter distance between CFP and YFP in the bound case than YC2.1 (69 Å versus 75 Å). The successful design of YC6.1 resulted in an improved dynamic range over that for YC2.1 and demonstrated the advantages of rational biosensor design. More importantly, the consistent results found from FPMOD simulation results with previous experimental data for YC2.1 and YC6.1 demonstrate that with the aid of computational modeling, potential biosensor candidates can be rationally designed and assessed through simulations prior to labor-intensive and time-consuming experimental studies.
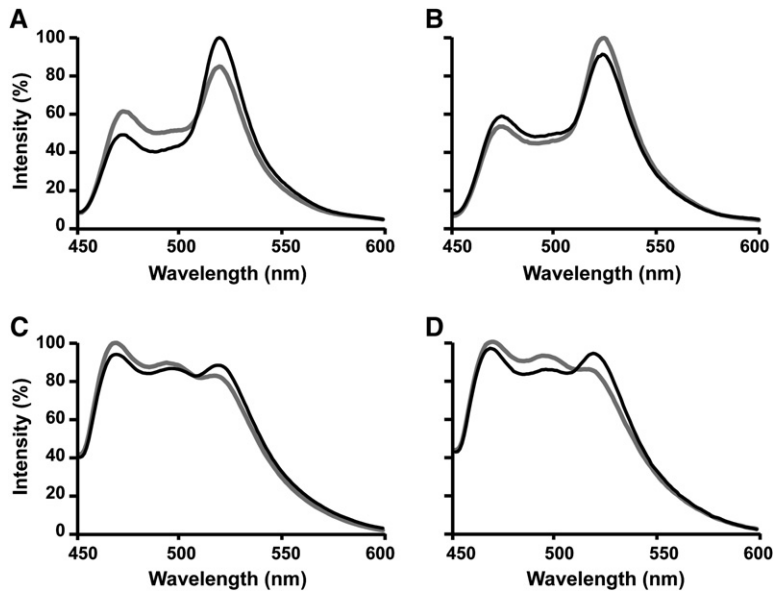
Certain YC2.1 Ca²⁺ Biosensors with Different Circularly Permutated Venus, cpVenus, Acceptors Can Have Dramatic FRET Efficiency Changes

By computational modeling of YC2.1 biosensors with cpVenus acceptors, FPMOD also confirmed that FRET efficiency changes are highly sensitive to relative spatial orientation. Circularly permuted proteins have been used to improve the dynamic range of FRET biosensors (Nagai et al., 2001, 2004; Nakai et al., 2001; Tallini et al., 2006). Nagai et al. used the YC2.1 biosensor as a template to optimize the relative orientation of the two fluorophores and their associated transition dipoles by fusing YFP at different angles. In addition to the original N terminus at residue Met1, new N termini were positioned at different sites on the β barrel, specifically at Thr49, Gln157, Asp173, Leu195, and Ile229. One of their constructs showed an increase in the emission ratio of Venus to CFP by nearly 600% with the saturation of Ca²⁺. This

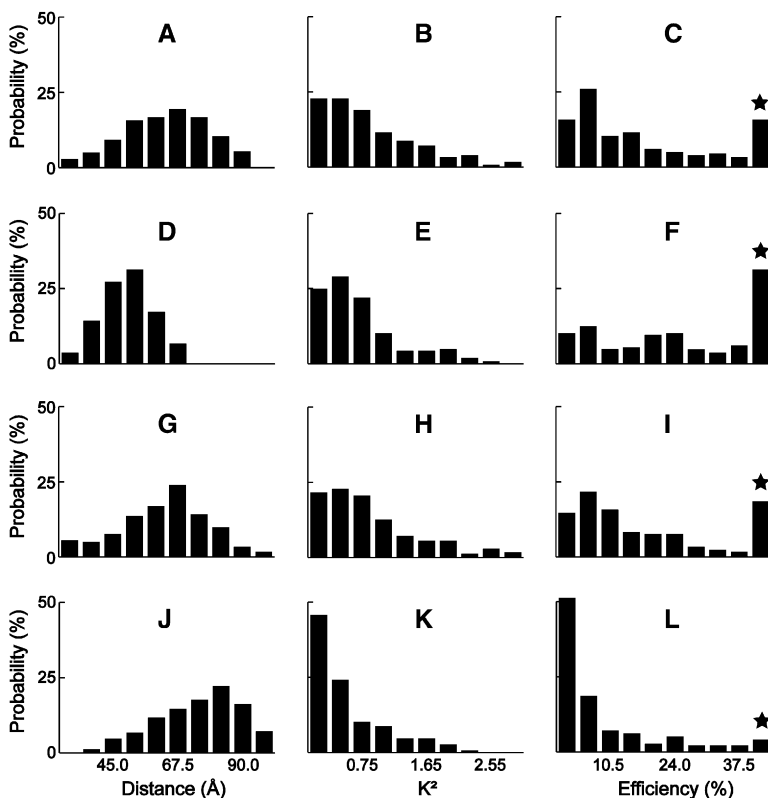6-fold dynamic range improvement allowed for higher-resolution imaging of subcellular Ca^{2+} changes in both cultured cells and in cells in the nervous system of transgenic mice (Nagai et al., 2004). It was found experimentally that different cpVenus acceptors displayed different emission-ratio changes, listed in descending order, in the presence of Ca^{2+}: cp173Venus (210%), cp157Venus (158%), original YC2.1 (122%), cp195Venus (102%), cp229Venus (75%), and cp49Venus (0%). FPMOD confirmed that the unbound FRET efficiencies of these biosensors were similar to those of YC2.1, because in the absence of Ca^{2+}, the domains have complete rotational freedom (data not shown). Furthermore, our FPMOD simulation results were consistent with the relative order of emission-ratio improvements (Table 1): cp173Venus (10%), cp157Venus (6.2%), original YC2.1 (5.9%), cp195Venus (3.0%), cp229Venus (1.3%), and cp49Venus (0.25%). In particular, simulation results confirmed that incorporating cp173Venus, rather than the other constructs, into the biosensor results in a significantly better improvement in FRET efficiency, and that incorporating the cp49Venus construct results in only a slight response to Ca^{2+}. When other cpVenus acceptors (cp58Venus, cp116Venus, cp135Venus, cp145Venus, and cp215Venus) were tested, several acceptors, namely, cp215Venus (5.1%), cp58Venus (4.9%), and cp145Venus (3.3%) demonstrated relatively good emission-ratio increases. Thus, these cpVenus acceptors might be good candidates for further experimental studies. The agreement between FPMOD simulation results and experimental data here indicates that FPMOD is versatile enough to improve dynamic range through the optimization of both distance and orientation factors of biosensors based on the Ca^{2+}-binding properties of the cytoplasmic CaM protein.

Ca^{2+} Biosensors Based on the Extracellular Epithelial Cadherin, Ecad, Repeats Show an Increase in FRET Efficiency after Binding to Ca^{2+}

A common shortcoming of biosensor constructs based on CaM as the Ca^{2+}-sensing component is their susceptibility to binding of endogenous CaM proteins to peptide regions, thus perturbing biosensor sensitivity to Ca^{2+} changes in vivo. For the same reason, there has been a concern that CaM-based biosensors may interfere with CaM signaling in cells (Heim and Griesbeck, 2004). One means of addressing these concerns is to reengineer the binding interface between CaM and the target peptide to prevent perturbations by excess endogenous CaM. This can be done by computationally designing complementary bumps and holes in peptides and CaM, respectively (Palmer et al., 2006). Alternatively, CaM can be replaced by other Ca^{2+}-sensitive proteins, including Troponin-C (Heim and Griesbeck, 2004; Mank et al., 2006) and Ecad, in novel biosensor constructs. In particular, the extracellular protein Ecad may not be susceptible to perturbations by cytoplasmic proteins in vivo. Ecad is a member of the Cadherin superfamily of Ca^{2+}-dependent cell-cell adhesion transmembrane glycoproteins. Structurally, Ecad has three major regions: a cytoplasmic domain, a transmembrane domain, and an extracellular

domain facilitating cell-cell adhesion. This extracellular region contains a tandem of five autonomously folding repeats of 100 amino acid residues. In the absence of Ca^{2+}, the extracellular region is floppy. In the presence of Ca^{2+}, linkers between two consecutive repeats bind three Ca^{2+} ions, which induces a conformational change in which the linkers become rigid and the repeats form homodimers (Alattia et al., 1999; Nagar et al., 1996).

Computational modeling with this class of FRET Ca^{2+} biosensors containing extracellular Ecad repeats predicted that the FRET efficiency should increase. The CEcad12Y and CEcad23Y biosensors were created and consisted of Ecad repeats 1–2 and 2–3 flanked by a CFP donor and YFP acceptor, respectively. Based on the solved atomic structure of Ecad repeats 1–2, FPMOD was used to generate models corresponding to the CEcad12Y biosensor before and after Ca^{2+} induction. To simulate the FRET efficiency change of the biosensor, FRET efficiency values were compared between the free and bound models. FPMOD predicted an increase from 3.1% to 4.5% in FRET efficiency upon binding of Ca^{2+}, which is an emission-ratio increase of 3.6% (Table 1). This is consistent with the in vitro finding that there was an increase in FRET emission ratio of 14% (Figure 2). Although simulations were not done for CEcad23Y due to the lack of a solved atomic structure for Ecad repeats 2–3, we suspect that it would behave similarly to CEcad12Y, as the structures are very similar. The FPMOD prediction of an increase in emission ratio for CEcad12Y is also consistent with the in vitro experimental increase of 13% for CEcad23Y. In addition, the counterintuitive finding that the distance shortened upon Ca^{2+} binding was also confirmed. After binding Ca^{2+}, the linker between Ecad repeats 1 and 2 becomes rigid and extended, suggesting a larger distance factor, and hence a lower FRET efficiency. However, simulated FRET efficiency values showed the opposite effect. Closer inspection of the bound models revealed that homodimerization of the bound case favored a shorter distance between the restrained CFP and YFP than the unbound case (91 Å and 85 Å, respectively). Homodimerization limits the rotational freedom of the biosensor models, as evident by the lower orientation values (from 0.59 to 0.39), and forces a closer distance between the CFP donor and YFP acceptor. These Ecad biosensor models generated by using FPMOD were capable of making nonintuitive predictions and were used to reveal the underlying mechanisms of the biosensor's conformational change.

In this paper, we have shown that FPMOD is an effective computational tool for the development and improvement of FRET biosensors. While it is difficult to determine the exact relationship between changes in FRET efficiency and emission ratio, the values should be directly proportional. FPMOD was used to evaluate the FRET efficiency and emission-ratio changes for both new and existing Ca^{2+} biosensor designs. For the YMLCKpC-CaM and YCKKpC-CaM biosensors, it showed that the former had an increase in FRET efficiency after Ca^{2+} induction, while the latter had a decrease. For existing biosensors,

YC6.1 and YC2.1, it showed that the larger dynamic range of the YC6.1 biosensor was predictable. Furthermore, it showed that the larger dynamic range of particular YC2.1 biosensors with cpVenus acceptors was also predictable. Lastly, it was used to design a class of Ca^{2+} biosensors (named CEcad12Y and CEcad23Y) based on epithelial Cadherin repeats, which showed an increase in FRET efficiency. All of these predictions were qualitatively validated with experimental data from our group and others. Therefore, this same approach can be applied to designing new biosensors whose protein structures as well as conformational changes due to specific bioactivities are known.

Further improvements to FPMOD might include a consideration of the effects of van der Waals interactions, electrostatic forces, and restricted dihedral angles on the conformational space. The inclusion of other effects, including heterodimerization of CFP and YFP, protein-protein docking statistical potentials, and solvation effects would further eliminate nonoptimal conformations, which would allow a better quantitative correlation between simulation and experimental results. Alternatively, experimental results could also be further refined through the use of anisotropy studies. Further studies are also required to determine the precise relationship between simulation FRET efficiency and experimental emission spectra.

Experimental Procedures
Calculating FRET Efficiency

$$E\% = \frac{R_0^6}{R_0^6 + R^6}, \tag{1}$$

$$R_0 = 9.78 \times 10^3 \times \left(Q_d \kappa^2 n^{-4} J\right)^{\frac{1}{6}} \text{Å}, \tag{2}$$

$$\kappa^2 = \left(\sin[\theta_D]\sin[\theta_A]\cos[\phi] - 2\cos[\theta_D]\cos[\theta_A]\right)^2. \tag{3}$$

FRET efficiency ($E\%$) is the percentage of energy transferred between a donor-acceptor fluorophore pair. This efficiency is a function of the Forster distance factor, R_o, the distance between the fluorophores, R, and the orientation factor, κ^2. In turn, the orientation factor depends on the angle between donor or acceptor fluorophore dipoles and the joining vector (θ_A and θ_D, respectively), as well as the angle between fluorophore pair planes (ϕ). A common assumed constant for κ^2 is 2/3, but this does not apply here because the linkers within the biosensors are not in isotropic motion upon Ca^{2+} binding (Dale et al., 1979; Hillel and Wu, 1976). Several relevant parameters are constants defined for the donor-acceptor pair used in the biosensor. For CFP and YFP, these constants are quantum yield (Q_D = 0.42), refractive index (n = 1.4), and overlap integral (J = 14,618e−13). The orientation of transition dipoles is defined with respect to PDB atom coordinates of the HETATM for CFP and YFP, from atom N15 to C4 and atom N3 to CZ, respectively. This assumed direction is kept consistent for all constructs simulated. For each conformation, the dipoles and related angles were determined from the PDB files and are used in Equations 1–3 to determine R, κ^2, and $E\%$.

Calculating the Emission Ratio from FRET Efficiency

$$E\% = \frac{F_D - F_{DA}}{F_D} = \frac{F_{NET}}{F_{NET} + F_{DA}}, \tag{4}$$

$$\frac{(F_D - F_{DA})}{Q_C} = \frac{SE}{Q_Y}, \tag{5}$$

$$SE = F_{A,FRET} - F_{A,CFP-OV} - F_{A,CFP-EX}, \tag{6}$$

$$F_{A,CFP-OV} = n_{CFP}F_{DA}, \tag{7}$$

$$EmR = \frac{F_{A,FRET}}{F_{DA}}, \tag{8}$$

$$EmR = \frac{-n_{CFP} - n_{CFP}E\% - (Q_Y/Q_C)E\%}{E\% - 1}. \tag{9}$$

A means of determining the FRET emission ratio from FRET efficiency has been developed previously by using Equations 4–6, where F_D is the donor CFP emission in the absence of the acceptor YFP, F_{DA} is the donor CFP emission in the presence of the acceptor YFP, F_{NET} is the net FRET signal, SE is the sensitized YFP emission due to FRET, Q_C is the quantum efficiency of the CFP donor, and Q_Y is the quantum efficiency of the YFP acceptor (Chen et al., 2005; Miyawaki and Tsien, 2000). Starting from these equations, we defined Equations 7–9 to calculate the emission ratio (EmR) from FRET efficiency values obtained through simulation. The sensitized YFP emission due to FRET, SE, is the total raw FRET signal ($F_{A,FRET}$) minus the overlap of donor emission with the acceptor emission ($F_{A,CFP-OV}$) and the acceptor emission due to direct excitation at the donor wavelength ($F_{A,CFP-EX}$). Given the 1:1 stoichiometry of CFP:YFP on these biosensors, the contribution of $F_{A,CFP-EX}$ is negligible. In addition, n_{CFP} is a spectral characteristic of the known shape of the CFP emission spectrum, where the contribution of the donor emission spectrum is roughly 0.7 of the total donor emission in the presence of the acceptor YFP. Q_y and Q_C are 0.76 and 0.42, respectively (Griesbeck et al., 2001).

Constructing a FRET Biosensor Model
Given the solved atomic structure of each domain of the biosensor (such as CFP, YFP, and the sensory proteins) in standard PDB format, FRET biosensor models are constructed by joining each domain with flexible linkers. Three subroutines of FPMOD are involved: residue insertion, residue deletion, and domain fusion. Residue insertion is used for adding linker residues. These linker residues are often introduced either from restriction enzyme sites used in the subcloning process or from the design process when it is desirable to lengthen the linkers for greater conformational freedom. In contrast, residue deletion is used to remove portions of the PDB file not required for the FRET biosensor model. After protein domains are necessarily truncated and linker residues are added, domain fusion is used to fuse the different domains and their linkers together.

Sampling of the Conformational Space of a FRET Biosensor Model
Once the FRET biosensor model is constructed, subroutines of FPMOD are then used to sample its conformational space. All domains of the FRET biosensor are treated as rigid bodies and are rotated around their flexible linkers. These flexible linkers are located between domains and do not form any secondary structures. For each residue in a linker, there are three torsional or dihedral angles, ψ, Φ, and ω. During rotation, all linker residues are randomly rotated such that all atoms of a linker residue preceding the N atom along the N-C_α bond are rotated by the torsional angle Φ. Next, all atoms after the C atom along the C_α-C bond are rotated by angle ψ. While the angles ψ and Φ do not have any restriction, and thus range from −180° to 180°, ω is fixed at 180°. This is a reasonable restriction since the *trans* configuration is most commonly found in nature. After all residues in the flexible linkers are randomly rotated and steric collisions are checked for, this corresponds to one possible conformation of the fusion protein. This model is then saved in PDB format, and the linker residue rotation process is repeated again until a representative number of models are generated to sufficiently span the conformational space. Tabulated values are averages over all possible conformations generated. The

number of models generated for each biosensor was deemed sufficient when doubling the number of models generated did not change the overall average obtained. In all of our tested cases, averages were calculated for 130 generated models.

Development of FPMODGui

To simplify the execution of FPMOD subroutines, a graphical user interface called FPMODGui was developed. It includes the following features: custom dialog boxes for each subroutine to ensure that the user will enter the necessary arguments, a Command History window to allow users to easily run recently used programs without having to retype the arguments, and an output window for viewing results. FPMODGui was developed by using the wxWindows toolkit and involved creating derived classes specific to FPMOD programs from generic classes found in the toolkit.

Constructing the YCKKpC-CaM and YMLCKpC-CaM Plasmids

Using the cassette-based technology described by Truong et al. (2003), the plasmids for expressing the YCKKpC-CaM and YMLCKpC-CaM biosensors were created with the combination of the plasmids pCFPtx (Truong et al., 2003), pYFPtx (Truong et al., 2003), pCKKtx, pMLCKtx, and pCaMtx. The latter three plasmids were created by, first, amplification from cDNA libraries and digestion with SpeI and XhoI. The fragments were then ligated into the SpeI and XhoI sites of pTriEx-3 (Novagen) to create the pCKKtx, pMLCKtx, and pCaMtx vectors, respectively. To construct the pYCKKpC-CaMtx and pYMLCKpC-CaMtx plasmids, three steps were involved. First, pCFPtx was digested with NcoI and NheI sites and then ligated into the NcoI and SpeI sites of pCaMtx to create the intermediate pCFP-CaMtx vector. Then, pYFPtx was digested with NcoI and NheI sites and ligated into the NcoI and SpeI sites of each of the pCKKtx and pMLCKtx vectors to create the intermediate vectors, pYFP-CKKtx and pYFP-MLCKtx, respectively. Finally, the pCFP-CaMtx vector was digested with SpeI and XhoI and then ligated into the NheI and XhoI sites of each of the pYFP-CKKtx and pYFP-MLCKtx vectors to create the final plasmids, pYCKKpC-CaMtx and pYMLCKpC-CaMtx, respectively. *E. coli* cells were transformed with these plasmids and were plated. A colony fluorescing both cyan and yellow was selected.

Constructing the CEcad12Y and CEcad23Y Plasmids

The plasmids for expressing CEcad12Y and CEcad23Y biosensors (pC12Ytx and pC23Ytx, respectively) were created with the combination of the following two plasmids: pCFPtx (Truong et al., 2003) and pCfvtx (Truong et al., 2003). To create the C12Y and C23Y biosensors, first the Ecad12 and Ecad23 fragments were amplified from cDNA libraries (Spring Bioscience) digested with SpeI-BglII and ligated into the SpeI-BglII sites of pCfvtx to construct the intermediate plasmids pEcad12Vtx and pEcad23Vtx. Finally, the pCFPtx plasmid was digested with NcoI-NheI and ligated into the NcoI-SpeI sites of pEcad12Vtx and pEcad23Vtx to construct the pC12Ytx and pC23Ytx plasmids, respectively. *E. coli* cells were transformed with pC12Ytx and pC23Ytx, and a single colony with both cyan and yellow fluorescence was selected.

Fluorescence Spectroscopy

Emission spectra of the biosensor constructs before and after Ca^{2+} saturation were recorded with a spectrophotometer (Shimadzu RF-5301PC) with an excitation wavelength of 440 nm. From the emission spectra, the biosensors displayed a CFP emission peak of 477 ± 1 nm and a YFP emission peak of 523 ± 1 nm.

REFERENCES

Alattia, J.R., Kurokawa, H., and Ikura, M. (1999). Structural view of cadherin-mediated cell-cell adhesion. Cell. Mol. Life Sci. *55*, 359–367.

Berridge, M.J., Lipp, P., and Bootman, M.D. (2000). The versatility and universality of calcium signalling. Nat. Rev. Mol. Cell Biol. *1*, 11–21.

Chen, H., Cohen, D.M., Choudhury, D.M., Kioka, N., and Craig, S.W. (2005). Spatial distribution and functional significance of activated vinculin in living cells. J. Cell Biol. *169*, 459–470.

Chiang, J.J., and Truong, K. (2006). Computational modeling of a new fluorescent biosensor for caspase proteolytic activity improves dynamic range. IEEE Trans. Nanobioscience *5*, 41–45.

Clegg, R.M. (1995). Fluorescence resonance energy transfer. Curr. Opin. Biotechnol. *6*, 103–110.

Dale, R.E., Eisinger, J., and Blumberg, W.E. (1979). The orientational freedom of molecular probes. The orientation factor in intramolecular energy transfer. Biophys. J. *26*, 161–193.

Griesbeck, O. (2004). Fluorescent proteins as sensors for cellular functions. Curr. Opin. Neurobiol. *14*, 636–641.

Griesbeck, O., Baird, G.S., Campbell, R.E., Zacharias, D.A., and Tsien, R.Y. (2001). Reducing the environmental sensitivity of yellow fluorescent protein. Mechanism and applications. J. Biol. Chem. *276*, 29188–29194.

Heim, N., and Griesbeck, O. (2004). Genetically encoded indicators of cellular calcium dynamics based on troponin C and green fluorescent protein. J. Biol. Chem. *279*, 14280–14286.

Hillel, Z., and Wu, C.W. (1976). Statistical interpretation of fluorescence energy transfer measurements in macromolecular systems. Biochemistry *15*, 2105–2113.

Ikura, M., Clore, G.M., Gronenborn, A.M., Zhu, G., Klee, C.B., and Bax, A. (1992). Solution structure of a calmodulin-target peptide complex by multidimensional NMR. Science *256*, 632–638.

Kuboniwa, H., Tjandra, N., Grzesiek, S., Ren, H., Klee, C.B., and Bax, A. (1995). Solution structure of calcium-free calmodulin. Nat. Struct. Biol. *2*, 768–776.

Li, I.T., Pham, E., and Truong, K. (2006). Protein biosensors based on the principle of fluorescence resonance energy transfer for monitoring cellular dynamics. Biotechnol Lett. *28*, 1971–1982.

Mank, M., Reiff, D.F., Heim, N., Friedrich, M.W., Borst, A., and Griesbeck, O. (2006). A FRET-based calcium biosensor with fast signal kinetics and high fluorescence change. Biophys. J. *90*, 1790–1796.

Miyawaki, A. (2003). Visualization of the spatial and temporal dynamics of intracellular signaling. Dev. Cell *4*, 295–305.

Miyawaki, A., and Tsien, R.Y. (2000). Monitoring protein conformations and interactions by fluorescence resonance energy transfer between mutants of green fluorescent protein. Methods Enzymol. *327*, 472–500.

Miyawaki, A., Llopis, J., Heim, R., McCaffery, J.M., Adams, J.A., Ikura, M., and Tsien, R.Y. (1997). Fluorescent indicators for Ca^{2+} based on green fluorescent proteins and calmodulin. Nature *388*, 882–887.

Miyawaki, A., Griesbeck, O., Heim, R., and Tsien, R.Y. (1999). Dynamic and quantitative Ca^{2+} measurements using improved cameleons. Proc. Natl. Acad. Sci. USA *96*, 2135–2140.

Nagai, T., Sawano, A., Park, E.S., and Miyawaki, A. (2001). Circularly permuted green fluorescent proteins engineered to sense Ca^{2+}. Proc. Natl. Acad. Sci. USA *98*, 3197–3202.

Nagai, T., Ibata, K., Park, E.S., Kubota, M., Mikoshiba, K., and Miyawaki, A. (2002). A variant of yellow fluorescent protein with fast and efficient maturation for cell-biological applications. Nat. Biotechnol. *20*, 87–90.

Nagai, T., Yamada, S., Tominaga, T., Ichikawa, M., and Miyawaki, A. (2004). Expanded dynamic range of fluorescent indicators for Ca(2+) by circularly permuted yellow fluorescent proteins. Proc. Natl. Acad. Sci. USA *101*, 10554–10559.

Nagar, B., Overduin, M., Ikura, M., and Rini, J.M. (1996). Structural basis of calcium-induced E-cadherin rigidification and dimerization. Nature *380*, 360–364.

Nakai, J., Ohkura, M., and Imoto, K. (2001). A high signal-to-noise Ca(2+) probe composed of a single green fluorescent protein. Nat. Biotechnol. *19*, 137–141.

Osawa, M., Tokumitsu, H., Swindells, M.B., Kurihara, H., Orita, M., Shibanuma, T., Furuya, T., and Ikura, M. (1999). A novel target recognition revealed by calmodulin in complex with Ca^{2+}-calmodulin-dependent kinase kinase. Nat. Struct. Biol. *6*, 819–824.

Palmer, A.E., Giacomello, M., Kortemme, T., Hires, S.A., Lev-Ram, V., Baker, D., and Tsien, R.Y. (2006). Ca^{2+} indicators based on computationally redesigned calmodulin-peptide pairs. Chem. Biol. *13*, 521–530.

Pozzan, T., Mongillo, M., and Rudolf, R. (2003). The Theodore Bucher lecture. Investigating signal transduction with genetically encoded fluorescent probes. Eur. J. Biochem. *270*, 2343–2352.

Rekas, A., Alattia, J.R., Nagai, T., Miyawaki, A., and Ikura, M. (2002). Crystal structure of venus, a yellow fluorescent protein with improved maturation and reduced environmental sensitivity. J. Biol. Chem. *277*, 50573–50578.

Tallini, Y.N., Ohkura, M., Choi, B.R., Ji, G., Imoto, K., Doran, R., Lee, J., Plan, P., Wilson, J., Xin, H.B., et al. (2006). Imaging cellular signals in the heart in vivo: cardiac expression of the high-signal Ca^{2+} indicator GCaMP2. Proc. Natl. Acad. Sci. USA *103*, 4753–4758.

Truong, K., and Ikura, M. (2001). The use of FRET imaging microscopy to detect protein-protein interactions and protein conformational changes in vivo. Curr. Opin. Struct. Biol. *11*, 573–578.

Truong, K., Sawano, A., Mizuno, H., Hama, H., Tong, K.I., Mal, T.K., Miyawaki, A., and Ikura, M. (2001). FRET-based in vivo Ca^{2+} imaging by a new calmodulin-GFP fusion molecule. Nat. Struct. Biol. *8*, 1069–1073.

Truong, K., Khorchid, A., and Ikura, M. (2003). A fluorescent cassette-based strategy for engineering multiple domain fusion proteins. BMC Biotechnol. *3*, 8.

Tsien, R.Y. (1998). The green fluorescent protein. Annu. Rev. Biochem. *67*, 509–544.

Wriggers, W., Mehler, E., Pitici, F., Weinstein, H., and Schulten, K. (1998). Structure and dynamics of calmodulin in solution. Biophys. J. *74*, 1622–1639.

Xu, X., Gerard, A.L., Huang, B.C., Anderson, D.C., Payan, D.G., and Luo, Y. (1998). Detection of programmed cell death using fluorescence energy transfer. Nucleic Acids Res. *26*, 2034–2035.